Biophysical Journal Volume 109 July 2015 319–329

Article

High Cholesterol Obviates a Prolonged Hemifusion Intermediate in Fast SNARE-Mediated Membrane Fusion

Alex J. B. Kreutzberger,[1] Volker Kiessling,[1] and Lukas K. Tamm[1,*]

[1]Center for Membrane Biology and Department of Molecular Physiology and Biological Physics, University of Virginia, Charlottesville, Virginia

ABSTRACT Cholesterol is essential for exocytosis in secretory cells, but the exact molecular mechanism by which it facilitates exocytosis is largely unknown. Distinguishing contributions from the lateral organization and dynamics of membrane proteins to vesicle docking and fusion and the promotion of fusion pores by negative intrinsic spontaneous curvature and other mechanical effects of cholesterol have been elusive. To shed more light on this process, we examined the effect of cholesterol on SNARE-mediated membrane fusion in a single-vesicle assay that is capable of resolving docking and elementary steps of fusion with millisecond time resolution. The effect of cholesterol on fusion pore formation between synaptobrevin-2 (VAMP-2)-containing proteoliposomes and acceptor t-SNARE complex-containing planar supported bilayers was examined using both membrane and content fluorescent markers. This approach revealed that increasing cholesterol in either the t-SNARE or the v-SNARE membrane favors a mechanism of direct fusion pore opening, whereas low cholesterol favors a mechanism leading to a long-lived (>5 s) hemifusion state. The amount of cholesterol in the target membrane had no significant effect on docking of synaptobrevin vesicles. Comparative studies with α-tocopherol (vitamin E) show that the negative intrinsic spontaneous curvature of cholesterol and its presumed promotion of a very short-lived (<50 ms) lipid stalk intermediate is the main factor that favors rapid fusion pore opening at high cholesterol. This study also shows that this single-vesicle fusion assay can distinguish between hemifusion and full fusion with only a single lipid dye, thereby freeing up a fluorescence channel for the simultaneous measurement of another parameter in fast time-resolved fusion assays.

INTRODUCTION

Membrane fusion is a fundamental biological process that constitutes a key step in exocytosis, viral entry, and development (1–4). One of the most frequently studied examples of membrane fusion is the fusion of synaptic vesicles with the presynaptic membrane that is catalyzed by the exocytotic SNAREs synaptobrevin-2 (VAMP-2), SNAP-25, and syntaxin-1a (5–8). The successful reconstitution of the vesicle (v-) SNARE synaptobrevin-2 and the target membrane (t-) SNAREs syntaxin-1a and SNAP-25 into opposing proteoliposomes provided the ultimate evidence that SNAREs alone are sufficient to fuse two distinct lipid bilayer membranes (9,10).

Membrane cholesterol is well known to be necessary for efficient exocytosis of synaptic vesicles in neurons (11–13) and cortical vesicles in sea urchins (14–16). Cholesterol has also been shown to recruit SNAREs and other secretory proteins into clusters in the plasma membranes of secretory cells (17–25). Although clearly dependent on cholesterol, these clustered protein domains differ from classical lipid rafts because they are not colabeled with typical raft markers (23). Cholesterol-dependent clusters of syntaxin-1a have also been found when syntaxin-1a was reconstituted into single-phase model membranes that were devoid of any lipid rafts (26,27). In addition, cholesterol is highly enriched in secretory vesicles (28–30) where it has been implicated in promoting membrane fusion (14,15). Previous reconstitution studies have shown that cholesterol accelerates SNARE-mediated fusion in lipid mixing assays (31,32), but the reasons for this acceleration were only partially addressed.

Although it is clear that cholesterol plays an important role in SNARE-mediated membrane fusion, the molecular mechanism by which it facilitates fusion remains elusive. Possible explanations for cholesterol's role in fusion might include the segregation of membrane proteins into domains (18–26,33,34), its ability to order membrane lipids (35,36) and changing membrane fluidity (37), as well as its potential to stabilize negatively curved lipid structures that are thought to be intermediates on the path to membrane fusion (38–40). These different modes of action of cholesterol could potentially apply to either increase the rates of docking of v- and t-SNARE vesicles or they could increase the intrinsic rates of fusion after cognate SNARE vesicles have docked.

Most fusion assays do not distinguish between vesicle docking and fusion. For example, the traditional bulk lipid mixing fusion assays that are commonly used to measure the activity of SNAREs record the combined evolution of docking and fusion (9,10). To distinguish between docking and fusion, single-vesicle fusion assays have been developed in several laboratories including our own (41–46). Because these assays discriminate between docking and fusion, intrinsic rates of fusion that occur on millisecond timescales

Submitted March 4, 2015, and accepted for publication June 8, 2015.

*Correspondence: lkt2e@virginia.edu

Editor: Joseph Falke.

0006-3495/15/07/0319/11 $2.00

http://dx.doi.org/10.1016/j.bpj.2015.06.022

can be measured directly and independent of docking that occurs on minute timescales and thereby dominates the measured rates in bulk fusion assays (44). Single-vesicle fusion approaches have proved useful in studying the effects of several membrane properties, including lipid composition and membrane curvature, on the rates and cooperativity of SNAREs in fusion (47,48). Therefore, these methods are well suited to examine the role of cholesterol on the initiation of fusion involving the mixing of lipids of the two apposed membranes, i.e., hemifusion, and the opening of the initial fusion pore on timescales that were not previously accessible. Applying this approach we find that cholesterol in the v- and t-SNARE membranes has little or no effect on docking, but increases the probability of proceeding quickly to full fusion thereby avoiding long-lived nonproductive hemifusion intermediates.

MATERIALS AND METHODS

Materials

The following materials were purchased and used without further purification: porcine brain L-α-phosphatidylcholine (bPC), porcine brain L-α-phosphatidylethanolamine (bPE), porcine brain L-α-phosphatidylserine (bPS), and 1,2-dioleoyl-sn-glycero-3-phosphoethanolamine-N-(lissamine rhodamine B sulfonyl) (Rh-DOPE) were from Avanti Polar Lipids (Alabaster, AL); 1,1'-dioctadecyl-3,3,3',3'-tetramethyl-indodicarbocyanine perchlorate (DiD) and sulforhodamine B were from Life Technologies (Frederick, MD); cholesterol, octyl-β-D-glucopyranoside (βOG), sodium cholate, 2,2',2'',2'''-(ethane-1,2-diyldinitrilo)tetraacetic acid (EDTA), and glycerol were from Sigma (St. Louis, MO); 3-[(3-cholamidopropyl)dimethylammonio]-1-propanesulfonate (CHAPS) were from Anatrace (Maumee, OH); 2-[4-(2-hydroxyethyl)piperazin-1-yl]ethanesulfonic acid (HEPES), potassium chloride (KCl) were from Research Products International (Mount Prospect, IL); chloroform, ethanol, Contrad detergent, all inorganic acids, bases, and hydrogen peroxide were from Fisher Scientific (Fair Lawn, NJ). Water was purified first with deionizing and organic-free 4 filters (Virginia Water Systems, Richmond, VA) and then with a NANOpure system from Barnstead (Dubuque, IA) to achieve a resistivity of 18.2 MΩ/cm.

SNARE protein expression and purification

SNARE proteins from *Rattus norvegicus* cloned in pET28a vector were expressed in *Escherichia coli* (*E. coli*) BL21(DE3) cells and purified as described in previous studies (49,50). The cysteine-free variant of SNAP-25A consisted of residues 1-206 and synaptobrevin-2 (syb2) constructs included residues 49-96, 1-96, or 1-117. The acceptor SNARE complex (ΔN complex) was a 1:1:1 ratio of syntaxin-1a (syx1a) (residues 183-288), SNAP-25, and syb49-96 and was purified from BL21(DE3) cells expressing all three proteins simultaneously, using the pET28a vector for SNAP-25A and the pETDuet-1 vector for syx183-288 and syb49-96 (51). The complex and full-length syb2 were purified by Ni^{2+}-NTA affinity chromatography followed by ion exchange chromatography using MonoQ or MonoS columns in the presence of 15 mM CHAPS (51).

Content- and lipid-labeled v-SNARE proteoliposomes

Syb2 proteoliposomes containing 100 mM sulforhodamine B and lipid compositions as above were prepared as previously reported in Kiessling et al. (52). The desired lipids mixed in organic solvents were evaporated under a stream of N_2 gas and placed under vacuum for 1 h. The dried lipid films were dissolved with 118 μL of 110 mM βOG in reaction buffer (20 mM HEPES, 150 mM KCl, pH 7.4) containing 100 mM sulforhodamine followed by the addition of appropriate volumes of synaptobrevin-2 to reach final volumes of ~180 μL and the desired lipid-to-protein ratio of 400. After 1 h of equilibration, the mixture was diluted to a final volume of 550 μL and a βOG concentration of ~24 mM with buffer containing 100 mM sulforhodamine B. This lipid/detergent/protein mixture was then loaded on a G-50 superfine Sephadex (GE Healthcare, Piscataway, NJ) column to remove free detergent and the labeled proteoliposomes were collected and used within 48 h. The average diameter of the resulting proteoliposomes was determined by electron microscopy (see Results).

Proteoliposome reconstitution with t-SNAREs

Proteoliposomes with ΔN complex were formed by rapid dilution and dialysis of sodium cholate from the respective proteins in detergent and bPC and cholesterol at the indicated ratios (44,53). The lipid-to-protein ratios were 1000. Lipids were mixed in chloroform and dried on the bottom of glass test tubes under a stream of nitrogen. The dried lipid films were dissolved with sodium cholate in reaction buffer (20 mM HEPES, 150 mM KCl, pH 7.4) followed by addition of the appropriate concentrations of protein and detergent-free buffer to obtain a solution of 25 mM sodium cholate in a final volume of 180 μL. The lipid, protein, and detergent mixtures were equilibrated at room temperature for 1 h and then diluted by addition of reaction buffer to a final volume of 550 μL to a concentration below the critical micellar concentration. Samples were then dialyzed overnight against 500 mL of reaction buffer at 4°C with one buffer change.

Acceptor t-SNARE complex-containing planar supported bilayers

Planar supported bilayers with reconstituted ΔN complex were prepared by the Langmuir-Blodgett/vesicle fusion technique as described in previous studies (44,54,55). Quartz slides were cleaned by boiling in Contrad detergent for 10 min, using hot bath-sonication while still in detergent for 20 min, and rinsing thoroughly with deionized water. Immediately before use, the slides were further cleaned for 1 to 2 min in an argon plasma sterilizer (Harrick Scientific, Ossining, NY). The first leaflet of the bilayer was prepared by Langumir-Blodgett transfer directly onto the quartz slide. A lipid monolayer of the desired bPC:cholesterol ratio was prepared on a pure water surface in a Nima 611 Langmuir-Blodgett trough (Nima, Conventry, UK) by applying the lipid mixture from a chloroform solution. After allowing the solvent to evaporate for 10 min, the monolayer was compressed at a rate of 10 cm^2/min to reach a surface pressure of 32 mN/m. After equilibration for 5 to 10 min, a clean quartz slide was rapidly (200 mm/min) dipped into the trough and slowly (5 mm/min) withdrawn, while a computer maintained a constant surface pressure and monitored the transfer of lipids with headgroups down onto the hydrophilic substrate. Proteoliposomes containing t-SNARE acceptor complex (77 μM total lipid in 1.3 mL) were added and incubated at room temperature for 2 h to introduce the protein complex and form the second leaflet of the supported bilayer. Excess unfused proteoliposomes were then removed by perfusion with 10 mL of reaction buffer containing 100 μM EDTA.

Cofloatation assay

The efficiency of protein insertion into liposomes was checked by a procedure similar to that described by Hernandez et al. (56). Liposomes containing t-SNAREs (50 μL) were mixed with 80% Nycodenz (Axis Shield, Dundee, Scotland) in a 250 μL centrifuge insert to make a 40% Nycodenz solution. Then 50 μL of 30% Nycodenz was layered onto the 40%

Nycodenz layer followed by a layer of 50 μL liposome buffer on top. The density gradient was centrifuged for 1.5 h in a Beckman TL-100 ultracentrifugre with a TLS55 rotor at 197,000 g and 4°C. Upon completion, 20 μL aliquots were carefully taken from the top of the gradient. Samples were then separated by SDS-PAGE and transferred to nitrocellulose filters (Invitrogen, Grand Island, NY); membranes were washed with Tris-buffered saline with 0.1% (v/v) Tween-20 (TBST, Invitrogen) and blocked in TBST with 2.5% (w/v) milk. Proteins were detected using an anti-SNAP-25 antibody (Synaptic Systems, Göttingen, Germany) and a horseradish peroxidase-conjugated monoclonal mouse secondary antibody that was visualized by chemiluminescence.

Total internal reflection fluorescence microscopy

Experiments were carried out on a Zeiss Axiovert 200 fluorescence microscope (Carl Zeiss, Thornwood, NY), equipped with a 63× water immersion objective (Zeiss; N.A. = 0.95) and a prism-based total internal reflection fluorescence (TIRF) illumination system. The beams of the 514 nm line of an argon ion laser (Innova 90C, Coherent, Palo Alto, CA), controlled through an acousto-optic modulator (Isomet, Springfield, VA), and a diode laser (Cube 640, Coherent) emitting light at 640 nm were directed (72° from the normal) into a prism above the quartz slide to illuminate the sample by total internal reflection with a characteristic penetration depth of ~102 and ~130 nm for the 514 and 647 nm lasers, respectively. The prism-quartz interface was lubricated with glycerol to allow easy translocation of the sample cell on the microscope stage. A OptoSplit (Andor-Technologies, South Windsor, CT) was used to separate the fluorescence from the lipid and soluble dyes. Fluorescence signals were recorded by an electron-multiplying charge-coupled device camera (iXon DV887ESC-BV, Andor, Belfast, UK). The EMCCD camera was cooled to -70°C and the electron gain factor was typically set to 240. The laser intensities, light-blocking shutters, and cameras were controlled by a homemade program written in LabVIEW (National Instruments, Austin, TX).

Single-vesicle fusion assay

Acceptor t-SNARE complex-containing planar supported bilayers were perfused with 3 mL syb2 proteoliposomes (~0.6 μM lipid) containing lipid and content labels. The fluorescence from the proteoliposomes was recorded with the 514 and 640 nm lasers using a EMCCD camera gain of 240. After focusing the microscope in the first 60 s after injecting the syb2 proteoliposomes, 5,000 images every 50.3 ms with 50 ms exposure times were taken and spooled directly to the hard drive. Two spooling sets were taken for each prepared bilayer and the averages of each spooling set were used to determine the efficiencies of hemifusion and direct full fusion. Although we used the ΔN acceptor complex that contains the C-terminal syb peptide to block formation of a nonproductive 2:1 complex, we have recently obtained similar results with a differently prepared 1:1 acceptor complex that lacks the syb peptide.

Single-vesicle fusion data were analyzed using a homemade program written in LabView (National Instruments). Stacks of images were filtered by a moving average filter. The intensity maximum for each pixel over the whole stack was projected on a single image. Vesicles were located in this image by a single-particle detection algorithm described in Kiessling et al. (57). The peak (central pixel) and mean fluorescence intensities of a 5 × 5 pixel^2 area around each identified center of mass were plotted as a function of time for all particles in the 5000 images of each series. The exact time points of docking and fusion were determined from the central pixel (44). Cumulative distributions were determined from the time of docking to the time of fusion for individual fusion events and the fusion efficiency was determined from the number of vesicles that underwent fusion compared with the total number of vesicles that docked.

Docking assay

Different amounts of proteoliposomes containing syb2 (54:20:5:20:1 of bPC:bPE:bPS:Chol:Rh-DOPE) made using the sodium cholate method described above were injected into the planar supported bilayer chamber and the total amount of fluorescence in the TIRF field was monitored over time. Early images were analyzed to determine the average fluorescence signal per liposome and this was used to convert fluorescence signal into number of liposomes bound.

Cryoelectron microscopy

Samples were applied to either c-flat or quantifoil holey carbon grids, blotted to near dryness, and plunged into a slurry of liquid ethane. Images were recorded at magnifications of 11,000× or 30,000× under low electron-dose conditions (~20 $e^-/Å^2$) using a 4k × 4k CCD camera (Gatan, Pleasanton, CA) fitted to a Tecnai F20 electron microscope.

Phosphate assay

Lipid concentrations were assayed by the Bartlett phosphate method (58) modified as described in Pokorny et al. (59). Appropriate volumes of standards and samples were pipetted and adjusted to 300 μL with distilled water. Then 700 μL of 70% $HClO_4$ was added. All tubes were covered with glass marbles and placed at 200°C for 30 to 60 min. Samples were then removed and allowed to cool, followed by addition of 2 mL 1% (w/v) ammonium molybdate and finally 2 mL 4% (w/v) ascorbic acid. The tubes were incubated at 37°C for 1 h, removed and cooled to room temperature before the absorbance was read at 700 nm.

Protein assay

The Pierce BCA protein assay kit from ThermoScientific was used according to manufacturer's directions.

RESULTS

Reconstituted synaptobrevin-2 proteoliposomes containing the membrane label DiD and the soluble content marker sulforhodamine B (52) dock to planar supported bilayers containing acceptor t-SNARE complexes in a SNARE-specific manner as was previously demonstrated (44,47,60). As shown in our earlier work, no docking (or fusion) of syb2 proteoliposomes was observed in the absence of either of the SNARE molecules or in the presence of the soluble syb1-96 inhibitor peptide (Fig. S1 in the Supporting Material). Docking was not dependent on the cholesterol concentration in the supported bilayer (Fig. S2). Based on the fluorescence signals that were extracted from 1.25 × 1.25 μm^2 regions of interest around docking liposomes we distinguish four characteristic types of events: Fig. 1 *I*, docking (without fusion); Fig. 1 *II*, hemifusion; Fig. 1 *III*, direct full fusion; and Fig. 1 *IV*, two-step fusion with a resolvable hemifusion intermediate. Events were classified as docking when syb2 proteoliposomes entered the TIRF field and remained stationary at the planar supported bilayer with constant fluorescent intensities of the membrane and content dyes (Fig. 1 *I*). Note that sulforhodamine B was included at self-quenching concentrations in these experiments

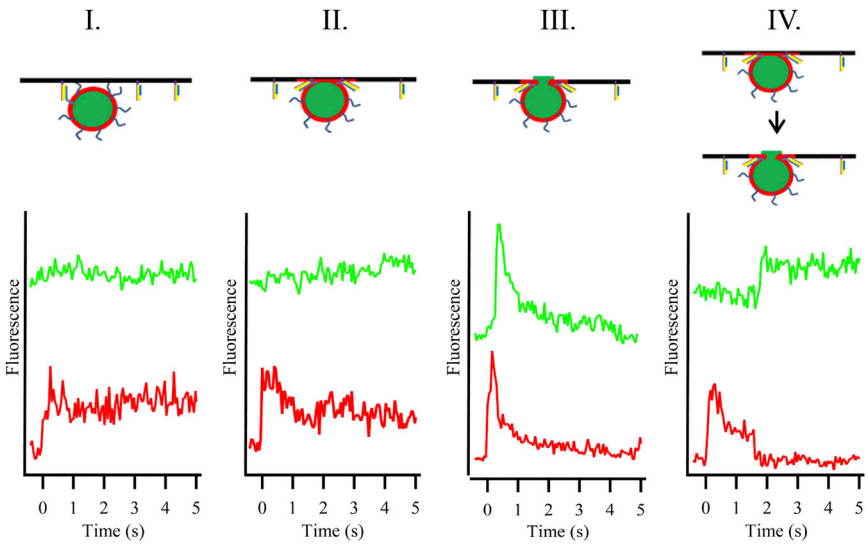

FIGURE 1 Four characteristic types of events observed in the single-vesicle fusion assay. The first row is a representative illustration of each type of event. The green (*upper*) traces are fluorescence intensity traces of the sulfurhodamine B content dye and the red (*lower*) traces are fluorescence intensity traces of the DiD membrane dye. (*I*) Docking of syb2 proteoliposomes is characterized by an increase in the membrane dye fluorescence caused by the liposome entering the TIRF field. This trace remains constant with no changes after the initial docking. Only a low background signal is observed for the content dye because sulforhodamine B is included at self-quenching concentrations in these experiments. (*II*) Hemifusion of syb2 proteoliposomes is characterized by a decrease of the membrane dye fluorescence to approximately half of the docked fluorescence signal. The content dye does not dequench in these events. (*III*) Direct full fusion of syb2 proteoliposomes is characterized by a decrease of the membrane dye fluorescence to baseline levels. The decrease of the membrane dye signal is paralleled by an increase of the content dye fluorescence that is attributable to dequenching, followed by a decrease attributable to diffusion of the dye into the cleft between the supported membrane and support. (*IV*) Occasionally, after a hemifusion event has been observed and the membrane dye fluorescence has leveled at approximately half-full intensity, a second decrease of the membrane dye fluorescence back to the background level occurs. This second drop of the signal is paralleled by a dequenching of the content dye. The four shown events are not plotted to scale attributable to differences in individual liposome sizes, their positions in the nonuniformly illuminated TIRF field and other optical and dye variations. To see this figure in color, go online.

resulting in fluorescence signals below the detection limit before fusion pore opening. Events were classified as hemifusion when the membrane dye fluorescence decreased to about half of its original intensity and the content dye fluorescence stayed constant (Fig. 1 *II*). Direct full fusion was characterized by dequenching of the content dye and a decrease of the membrane dye signal to baseline levels (Fig. 1 *III*). Subsequently the content dye decreases indicating diffusion out of the region of interest within the narrow cleft between the quartz support and planar bilayer at rates slower than those described for vesicle bursting events (61,62). No other events were regularly observed. To prove that fusion can be readily distinguished from vesicle bursting, we performed experiments, in which we deliberately let sulforhodamine B-loaded vesicles burst on a lipid monolayer-coated quartz slide. Fig. S3 shows that bursting events exhibit much faster three-dimensional dye diffusion than controlled fusion events with pseudo–two-dimensional dye diffusion in the cleft. Therefore, the two processes can be readily distinguished.

The reason for the lipid signal to decrease only half-way in hemifusion and all the way in full fusion is that only the proximal leaflets of the fusing lipid bilayers merge in hemifusion, but both leaflets merge and the lipids eventually diffuse into the large reservoir of the planar supported bilayer in full fusion. Events, in which the membrane fluorescence decays to the baseline in two distinct steps were classified as two-step hemifusion to full fusion processes (Fig. 1 *IV*). These events were rather rare (less than 2% of all observed events). In some cases the content dye dequenching was not followed by a decay of the fluorescence to the baseline level (Fig. 1 *IV*). Fig. S4 shows a relatively rare example of direct full fusion with the dequenched content dye not leaving the location of the liposome and an example of a two-step fusion event, in which the content fluorescence decreased to the baseline within 1 s. The same four characteristic membrane dye traces have been previously observed in the case of DNA-lipid conjugate mediated membrane fusion (63). Entire recording times of typical docking and fusion traces are shown in Fig. S5.

The fusion of syb2 proteoliposomes with a constant 20 mol % concentration of cholesterol was monitored with increasing concentrations of cholesterol in the planar supported target membrane. Changes in target membrane cholesterol did not affect overall protein concentrations or their efficiencies of insertion into the proteoliposomes that were used to form the planar supported bilayers (Fig. S6). In the absence of cholesterol, ~80% of all fusion events were hemifusion events. However, when cholesterol was increased in the target membrane, direct full fusion events increased gradually until they reached ~80% of all fusion events at 40 mol % cholesterol (Fig. 2 *a*). We extracted the delay times between docking and the onset of fusion or hemifusion for all events. Normalized cumulative distribution functions (CDFs) of these time delays were constructed as shown in Fig. 2, *b* and *c*, respectively. These are kinetic curves representing the fusion and hemifusion reactions, respectively, without any contribution from vesicle docking. The kinetic data were fit to several

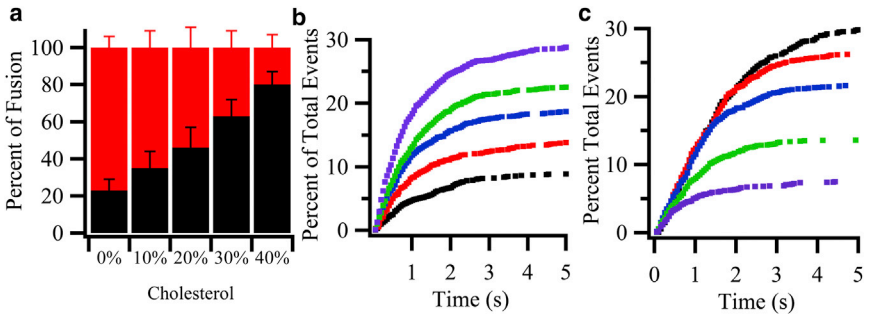

FIGURE 2 Summary of direct full fusion and hemifusion events obtained from single-vesicle fusion assays as a function of cholesterol in the planar supported target membrane. (*a*) Relative fractions of direct full fusion (*black*) and hemifusion (*red* or *gray*) at different mol % of cholesterol in the planar target membrane after 5 s. The numerical values are 23 ± 6%, 35 ± 9%, 46 ± 11%, 63 ± 9%, and 80 ± 7% full fusion and 77 ± 6%, 65 ± 9%, 54 ± 11%, 37 ± 9%, and 20 ± 7% hemifusion of the total number of fusion events (total numbers are shown in Table 1), respectively, at 0, 10, 20, 30, and 40 mol % cholesterol. (*b*) Cumulative distribution functions of direct full fusion events normalized to the efficiencies of total docking events, which were 9 ± 3%, 14 ± 4%, 19 ± 6%, 22 ± 5%, and 29 ± 5% for (*from bottom to top*) 0 (*black*), 10 (*red*), 20 (*blue*), 30 (*green*), and 40 (*purple*) mol % cholesterol, respectively, in the planar target membrane. (*c*) Cumulative distribution function of hemifusion events normalized to the efficiencies of total docking events, which were 30 ± 6%, 26 ± 6%, 22 ± 6%, 14 ± 5%, and 7 ± 4% for (*from top to bottom*) 0 (*black*), 10 (*red*), 20 (*blue*), 30 (*green*), and 40 (*purple*) mol % cholesterol, respectively, in the planar target membrane. To see this figure in color, go online.

models including the following very simple first-order rate law:

$$A \rightarrow B$$

and the following rate law with two consecutive steps:

$$A \rightarrow B \rightarrow C$$

characterized by two different rate constants, k_1 and k_2. The single-step rate law did not result in good fits for all experimental data, whereas the two-step rate law reproduced the experimental data very well. More complex kinetic models were not needed to explain the data. A summary of all recorded events under different conditions is shown in Table 1. The rate constants derived from the kinetic fits of the two-consecutive step model are shown in Table 2. The processes are characterized by a slower rate of ~1 s^{-1} that is quite independent of the type of fusion and the cholesterol concentration and a faster rate on the order of 3 to 20 s^{-1} that is a little more, but not strongly process- and cholesterol-dependent. The kinetic models do not a priori assign the order of the fast and slow processes in the above scheme.

The single events characterized in Fig. 1 suggest that the intensity traces originating from the membrane dye fluorescence might be sufficient to distinguish between hemifusion and full fusion. To further verify this we measured the fluorescence intensity of the membrane dye before docking, after docking, and after fusion (hemi- or full) for all fusion events of the series with increasing cholesterol concentration in the supported target membrane (Fig. 2). These data were used to determine the percentage of membrane dye fluorescence that had diffused into the planar membrane after fusion for each cholesterol condition (Fig. 3, *a–e*). The ratios of direct full to hemifusion events were calculated from these histograms and compared with those obtained from the content mixing assay shown in Fig. 2 *a*. The results obtained by the two independent methods correlated very well as shown in Fig. 3 *f*, proving that hemi- and full fusion can be readily distinguished in these experiments by monitoring the evolution of the lipid dye fluorescence only.

To determine if cholesterol in the vesicle membrane has similar effects on hemi- and full fusion as in the planar target membrane, we changed the cholesterol concentration in syb2 proteoliposomes from 0 to 40 mol % while keeping the cholesterol concentration in the planar target membrane constant at 20 mol %. Because membrane curvature can influence the efficiency and kinetics of SNARE-mediated membrane fusion (48), we first examined if cholesterol changed the size of the reconstituted syb2 vesicles. Indeed, when the cholesterol concentration was increased, the mean diameter of the proteoliposomes as determined by

TABLE 1 Summary of events at different cholesterol concentrations in the planar supported bilayer

Cholesterol (%)	Total No. of Direct Full Fusion Events	Total No. of Hemifusion Events	Total No. of Docked Liposomes	No. of Experiments
0	132	437	1418	8
10	253	472	1855	12
20	370	412	1973	7
30	537	313	2520	8
40	604	142	2105	7

These data were used to generate Fig. 2 *a* and to normalize Fig. 2, *b* and *c*. The error bars in Fig. 2 *a* represent the averages of all experiments under each condition.

TABLE 2 Rate constants (k (s^{-1})) derived from fits of the data of Fig. 2, *b* and *c*, to the two-step model of direct full fusion and hemifusion

	Direct Full Fusion		Hemifusion	
Cholesterol (%)	k_1 (s^{-1})	k_2 (s^{-1})	k_1 (s^{-1})	k_2 (s^{-1})
0	0.73 ± 0.06	18 ±7	0.75 ± 0.06	2.9 ± 0.4
10	1.00 ± 0.06	16 ± 4	0.80 ± 0.05	4.6 ± 0.6
20	1.00 ± 0.04	22 ± 5	0.91 ± 0.05	6.3 ± 0.9
30	0.96 ± 0.04	15 ± 2	0.97 ± 0.06	10 ± 2
40	1.17 ± 0.04	13 ± 2	1.4 ± 0.1	11 ± 3

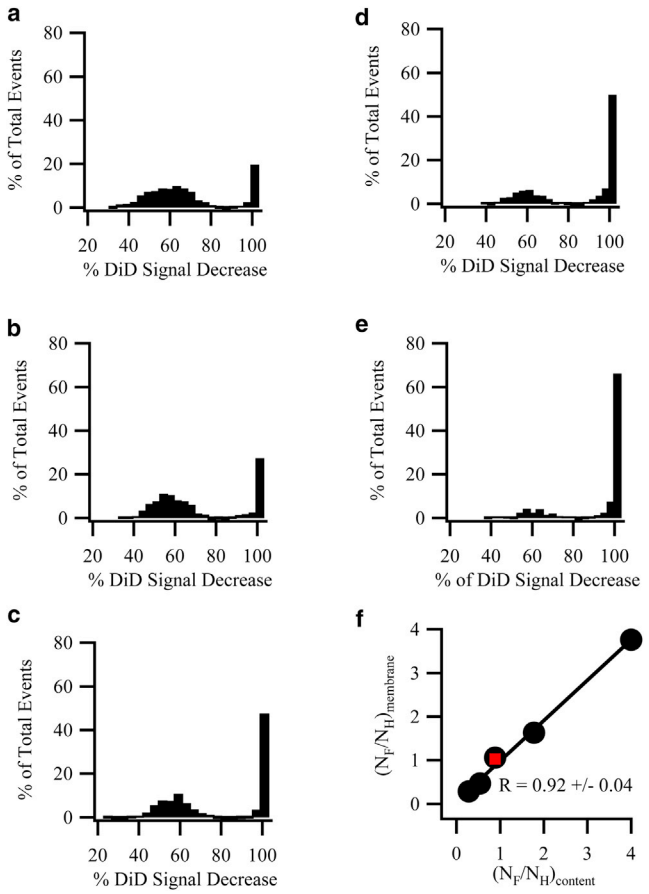

FIGURE 3 Histograms of DiD label diffusing into the planar target membrane after single syb2 proteoliposome fusion events with (*a*) 0, (*b*) 10, (*c*) 20, (*d*) 30, and (*e*) 40 mol % cholesterol in the planar target membranes. Fluorescence intensities of each fusion event were measured before syb2 proteoliposome docking, after docking, and after fusion. (*f*) Correlation of the percent full fusion (measured by content dye release) from Fig. 2 *a* and the percent membrane dye diffusion into the planar membrane. The correlation coefficient is 0.92 ± 0.04. The red (or *gray*) square represents an independent experiment using 20% cholesterol where only a rhodamine-DOPE membrane label was used instead of the DiD membrane and sulforhodamine B content labels, indicating that the DiD signal is not contaminated by bleed-through from sulforhodamine B fluorescence. To see this figure in color, go online.

cryoelectron microscopy increased from ~25 nm in the absence of cholesterol to ~40 nm at 20 and 40 mol % cholesterol (Fig. 4, *a–c*). More examples of cryoelectron microscopy images are shown in Fig. S7. The influence of cholesterol in the syb2 proteoliposomes on the fusion efficiencies was similar to the ones observed when cholesterol was increased in the acceptor complex-containing target membrane. The proportion of direct full fusion events increased substantially at the expense of long-lived hemifusion events when cholesterol was increased in the syb2 proteoliposomes (Fig. 4 *d*). The normalized cumulative distribution functions of the fusion delay times for direct full fusion and hemifusion are shown in Fig. 4, *e* and *f*, respectively. A summary of all recorded events under different conditions is shown in Table 3. The kinetic data could again be best fitted to the consecutive-step model and the derived kinetic rate constants are shown in Table 4. As with cholesterol in the planar target membrane, the two rates were on the orders of 1 s^{-1} and 10 s^{-1}.

Our result that increased cholesterol concentrations in the target and vesicle membranes promote direct full fusion vis-à-vis hemifusion indicates that cholesterol plays an important role in fusion pore opening. A large body of previous work has suggested that membrane components that alter the intrinsic spontaneous curvature of membranes are very important contributors of membrane fusion (3,15). Because cholesterol is well known to induce negative spontaneous curvature (0.040 $Å^{-1}$) in lipid bilayers (39), we wanted to know if this property of cholesterol is critical for suppressing long-lived hemifusion and promoting direct full fusion events. α-Tocopherol (vitamin E) is an even stronger negative spontaneous curvature-promoting agent (0.073 $Å^{-1}$) in lipid bilayers than cholesterol (15,64). Because α-tocopherol provides on a molar basis ~1.82 times more negative intrinsic spontaneous curvature to a lipid bilayer than cholesterol, we added 10 and 20 mol % α-tocopherol to the supported planar target membrane and used the single-vesicle fusion assay to measure the fusion of syb2 proteoliposomes that contained the standard 20 mol % cholesterol. As with cholesterol, the proportions of direct full fusion to hemifusion increased as the amount of α-tocopherol in the target membrane was increased (Fig. 5 *a*). Indeed, when compared at the same mol fraction, α-tocopherol was about twice as powerful as cholesterol in favoring direct full fusion over long-lived hemifusion. Specifically, the direct full fusion fractions for α-tocopherol over cholesterol were ~1.4 and ~1.7 at 10 and 20 mol % of the two curvature agents, respectively. This result strongly suggests that the negative intrinsic spontaneous curvature of cholesterol is primarily responsible for its role in promoting direct full fusion. However, when the fusion kinetics are compared, the rates of hemifusion and direct full fusion were both slower in the presence of α-tocopherol than in the presence of cholesterol (Fig. 5, *b* and *c*), indicating that the more compact cholesterol fits better into transition states of fusion than the more flexible α-tocopherol. The kinetics with α-tocopherol are not well described by the single or the two-consecutive-step kinetic models, and we did not attempt to fit these data. A summary of all recorded events under different conditions with α-tocopherol is shown in Table 5.

DISCUSSION

Cholesterol is enriched in synaptic vesicle and presynaptic plasma membranes and modulates the localization and function of many secretory proteins including SNAREs (18,21,26,32,65) synaptophysin (29,65,66), synaptotagmins (67,68), and synaptic calcium channels (19,69). Moreover,

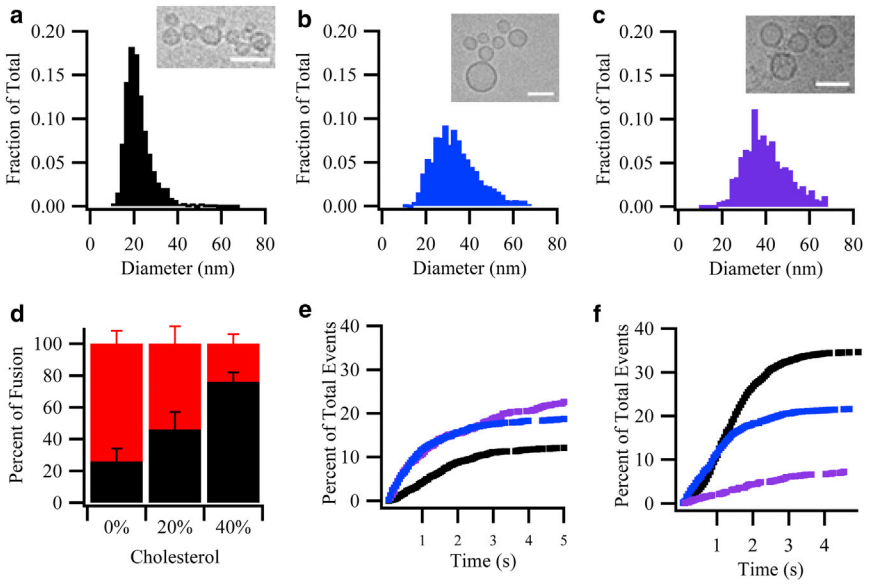

FIGURE 4 Summary of direct full fusion and hemifusion events obtained from single-vesicle fusion assays as a function of cholesterol in syb2 proteoliposome membrane. (*a–c*) Size distributions of syb2 proteoliposomes measured by cryoelectron microscopy for proteoliposomes containing (*a*) 0, (*b*) 20, and (*c*) 40 mol % cholesterol. Insets are example images for each condition with scale bars of 50 nm. (*d*) Relative fractions of direct full fusion (*black*) and hemifusion (*red* or *gray*) at different mol % of cholesterol in the syb2 proteoliposome membrane after 5 s. The numerical values are 26 ± 8%, 46 ± 11%, and 76 ± 6% of direct full fusion and 74 ± 8%, 54 ± 11%, and 24 ± 6% hemifusion of the total number of fusion events (total numbers are shown in Table 3), respectively, at 0, 20, and 40 mol % cholesterol. (*e*) Cumulative distribution function of direct full fusion events normalized to the efficiencies of total docking events, which were 12 ± 4%, 19 ± 6%, and 23 ± 2% of total number of events for (*from bottom to top*) 0 (*black*), 20 (*blue*), and 40 (*purple*) mol % cholesterol, respectively, in the syb2 proteoliposome membrane. (*f*) Cumulative distribution function of hemifusion events normalized to the efficiencies of total docking events, which were 35 ± 7%, 22 ± 6%, and 7 ± 2% hemifusion of the total number of events for (*from top to bottom*) 0 (*black*), 20 (*blue*), and 40 (*purple*) mol % cholesterol, respectively, in the syb2 proteoliposome membrane. To see this figure in color, go online.

numerous reports have shown that cholesterol plays an important role in synaptic vesicle fusion (11–13). However, the precise molecular mechanism, by which cholesterol acts on synaptic vesicle fusion, has not been elucidated. Because it is now well established that SNAREs are the central players in synaptic vesicle fusion, the role of cholesterol on the molecular mechanism of SNARE-mediated fusion is best studied in a reconstituted system. The reconstituted fast single-vesicle fusion system that we have developed is ideal for this purpose because it readily distinguishes between vesicle docking and fusion (44), their dependence on different lipid components (47), as well as its ability to distinguish between hemi- and full fusion (this study). This reconstituted system also recapitulates the fusion of purified synaptic vesicles (52). Investigating the effects of cholesterol on fusion in a reconstituted system allowed us to directly assess its effects on SNARE-mediated membrane fusion without confounding additional effects on other proteins that may be present in cellular systems. As shown in Fig. S2, we did not detect any significant differences in docking when cholesterol concentrations were changed in the target membrane and we do not anticipate that this would change by increasing cholesterol in the vesicle membrane.

Using the reconstituted single-vesicle fusion assay, we found that hemifusion is the dominant mode of fusion at low cholesterol concentrations and that direct full fusion dominates at increased concentrations of cholesterol that best represent the physiological situation. Our results also show that physiological cholesterol is needed in both the syb2 vesicle and the t-SNARE membrane to support direct full fusion. When cholesterol is lowered in either membrane, long-lived (>5 s) hemifusion intermediates develop that only rarely proceed to a fully fused state. We thus consider most of these hemifused events as nonproductive side reactions that the cell avoids by incorporating enough cholesterol into the synaptic vesicle and presynaptic target membranes.

It is noteworthy that the fusion kinetics were best fit with a model of two consecutive steps for both the direct full fusion and the hemifusion cases. The kinetic fits of hemifusion and direct full fusion are both best characterized by a slow rate

TABLE 3 Summary of events at different cholesterol concentrations in the syb2 proteoliposomes

Cholesterol (%)	Total No. of Direct Full Fusion Events	Total No. of Hemifusion Events	Total No. of Docked Liposomes	No. of Experiments
0	185	418	1524	5
20	400	412	1973	7
40	243	78	1073	5

These data were used to generate Fig. 4 *d* and to normalize Fig. 4, *e* and *f*. The error bars in Fig. 4 *d* represent the averages of all experiments under each condition.

TABLE 4 Rate constants (k (s^{-1})) derived from fits of the data of Fig. 4, *e* and *f*, to the two-step model of direct full fusion and hemifusion

	Direct Full Fusion		Hemifusion	
Cholesterol (%)	k_1 (s^{-1})	k_2 (s^{-1})	k_1 (s^{-1})	k_2 (s^{-1})
0	0.9 ± 0.2	1.7 ± 0.4	1.16 ± 0.03	–
20	1.00 ± 0.04	22 ± 5	0.91 ± 0.05	6.3 ± 0.9
40	0.70 ± 0.04	33 ± 17	0.31 ± 0.07	8 ± 4

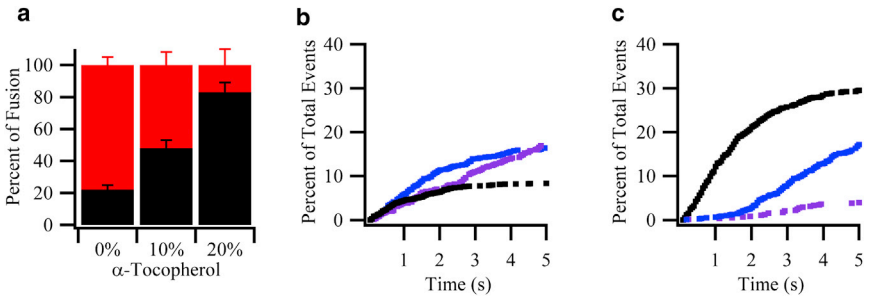

FIGURE 5 Summary of direct full fusion and hemifusion events obtained from single-vesicle fusion assay as a function of α-tocopherol in the planar supported bilayer. Syb2 proteoliposomes were composed of bPC:bPE:bPS:chol:DiD (53:20:5:20:2) as in the experiments reported in Fig. 2. (*a*) Relative fractions of direct full fusion (*black*) and hemifusion (*red* or *gray*) of the total number of fusion events after 5 s (total numbers are shown in Table 5). The numerical values are 22 ± 3%, 50 ± 5%, and 79 ± 5% direct full fusion and 78 ± 6%, 50 ± 3%, and 21 ± 3% for 0, 10, and 20 mol % α-tocopherol, respectively. (*b*) Cumulative distribution function of direct full fusion events normalized to the efficiencies of total docking events, which were 8 ± 3%, 17 ± 5, and 15 ± 5% for (*from bottom to top*) 0 (*black*), 10 (*blue*), and 20 (*purple*) mol % α-tocopherol, respectively. (*c*) Cumulative distribution function of hemifusion events normalized to the efficiencies of total docking events, which were 29 ± 6%, 17 ± 3%, and 4 ± 3% for (*from top to bottom*) 0 (*black*), 10 (*blue*), and 20 (*purple*) mol % α-tocopherol, respectively. To see this figure in color, go online.

constant of ~1 s^{-1} and a faster rate constant of ~18 s^{-1} in direct full fusion or ~8 s^{-1} in hemifusion (Table 2). We thus propose a model that combines the direct full fusion and hemifusion reactions into the following kinetic scheme:

$$V + T \begin{matrix} \nearrow \; I_F \rightarrow F \\ \searrow \; I_H \rightarrow H \end{matrix},$$

where vesicle V and target T membranes proceed to an intermediate I that then develops either into a full fusion pore F or a long-lived hemifusion state H. Our experiments do not allow us to assign the faster or slower rates to the first or second steps in the above reaction scheme. However, irrespective of whether the process leading to the intermediates is represented by the faster or slower rates, the time constant for populating the intermediate is at least 100 ms and perhaps as long as 1 s, i.e., long enough that we should see some lipid dye transfer if it had occurred during this time. Since our frame resolution in these experiments was 50 ms and we did not see any lipid transfer, the intermediates that we observe in either path cannot be a lipid stalk. More likely, it involves some rearrangement of the SNAREs that precedes the development of the stalk. However, once such a stalk has developed, it progresses directly into a full fusion pore at high cholesterol or into a dead-end hemifused state at low cholesterol on a timescale that must be faster than 50 ms, i.e., the time resolution of our experiments.

TABLE 5 Summary of events at different α-tocopherol concentrations in the planar supported bilayer

α-Tocopherol	Direct Full Fusion Events	Hemifusion Events	Total Events	No. of Bilayers Examined
0	92	332	1185	5
10	131	134	890	5
20	99	24	650	5

These data were used to generate Fig. 5 *a* and to normalize Fig. 5, *b* and *c*. The error bars in Fig. 5 *a* represent the averages of all experiments under each condition.

Chang et al. (31) measured the effects of cholesterol on fusion and SNARE assembly by bulk lipid mixing and a Förster resonance energy transfer assay, respectively. They concluded that cholesterol accelerated the kinetics of hemifusion but had only mild effects on fusion pore opening. These results are not directly comparable with ours because they measure the combination of docking and fusion on timescales of minutes and because they do not query the relative fractions of hemi- and full fusion. However, the different observations can be reconciled when one realizes that some fraction in the population of vesicles that are measured in the bulk fusion assay may proceed rapidly to hemifusion and eventually convert to full fusion after resting at a hemifused intermediate for a long time. In another study, Tong et al. (32) showed that cholesterol in the v-SNARE membrane caused a greater increase in the rate of lipid mixing than cholesterol in the t-SNARE membrane. The authors concluded that this increase was because of a structural rearrangement of syb2, but not the acceptor t-SNARE complex. We think that cholesterol might also change the partitioning of the N-terminal half of the SNARE motif of syb2 between the surface of the vesicle bilayer and the surrounding solution that we observed to be highly dependent on membrane curvature (70). Based on fluorescence measurements, this partitioning is not expected to happen with the preassembled acceptor t-SNARE complex in the target membrane (71). It is also possible that the syb2 SNARE motif partitioning between the membrane surface and solution takes place on a timescale that would appear as two distinct populations in our fast single-vesicle fusion assay, but an average in the much slower bulk fusion assay. This timescale difference may well explain why the effects of cholesterol are symmetric in our single-vesicle fusion assay, but appear asymmetric in the bulk fusion assay.

Our result that α-tocopherol causes very similar shifts in the relative proportions of direct full fusion and prolonged

hemifusion events at equivalent levels of induced negative spontaneous curvature argues strongly in favor of cholesterol causing this shift because of its ability to induce such curvature in lipid bilayers. Because α-tocopherol does not order lipids, change their fluidity, or induce raftlike domains in complex lipid mixtures, it is unlikely that these effects of cholesterol contribute significantly to the shift from the hemifusion to the full fusion pathway. The requirement for negative intrinsic spontaneous curvature in membrane fusion is usually explained by the fact that this curvature stabilizes a lipid stalk intermediate on the way to forming a fusion pore (3,72,73). We consider it very likely that the lipid stalk promoted by cholesterol (and α-tocopherol) represents a short-lived and kinetically invisible transition state on the path to open the fusion pore. Because the time resolution in our experiments was 50 to 100 ms, the lifetime of the stalk must be less than ~50 ms in our experiments. On the other hand, in the absence of cholesterol, the energy of the stalk transition state that leads to full fusion is high so that the membranes proceed to a different, relatively stable hemifusion state, which may entail an extended hemifusion diaphragm and which may or may not break to form a fusion pore at a later stage (3,74). Because membranes with α-tocopherol fuse more slowly than membranes with cholesterol, factors other than curvature also contribute to the energy barriers for transitioning directly into the fusion pore and the relatively stable hemifusion diaphragms.

This work has also revealed that a content dye is not required in our single-vesicle fusion assay to distinguish between hemi- and full fusion. Other single-vesicle fusion assays that have been developed rely on a second dye to distinguish between hemi- and full fusion (75,76). Rather, our assay relies on a change in polarization to indicate the beginning of fusion (60) and the fact that hemi- and fully fused states can be readily distinguished from the different levels of lipid dye fluorescence. This frees up a fluorescence channel on the microscope for monitoring other parameters at the single-vesicle level while not giving up the ability to simultaneously determine whether fusion has proceeded to a hemifused or fully fused state. This feature will become very useful in the future for measuring in real time changes in the conformational or assembly states of the fusion proteins as fusion proceeds.

SUPPORTING MATERIAL

Supporting Materials and Methods and seven figures are available at http://www.biophysj.org/biophysj/supplemental/S0006-3495(15)00604-9.

AUTHOR CONTRIBUTIONS

A.J.B.K. designed the research, performed the research, analyzed the data, and wrote the article; V.K. designed the research, contributed analytical tools, and analyzed the data; and L.K.T. designed the research, analyzed the data, and wrote the article.

ACKNOWLEDGMENTS

This work was supported by grant P01 GM72694 from the NIH. We thank Barbie Ganser-Pornillos and the Molecular Electron Microscopy Core facility at the University of Virginia (supported by the School of Medicine and built with NIH grant G20-RR31199) for the cryoelectron microscopy images of syb2 proteoliposomes. Kasia Janiszewska is acknowledged for her early work on this project. We thank David Castle and Candice Inouye for help with the Western blots, Matias Hernandez for assistance with the cofloatation assay and comments on initial observations of hemifusion, Binyong Liang for assistance with SNARE protein purification, and David Cafiso, David Castle, and Peter Kasson for numerous helpful discussions.

REFERENCES

1. Tamm, L. K., J. Crane, and V. Kiessling. 2003. Membrane fusion: a structural perspective on the interplay of lipids and proteins. *Curr. Opin. Struct. Biol.* 13:453–466.
2. Martens, S., and H. T. McMahon. 2008. Mechanisms of membrane fusion: disparate players and common principles. *Nat. Rev. Mol. Cell Biol.* 9:543–556.
3. Chernomordik, L. V., and M. M. Kozlov. 2008. Mechanics of membrane fusion. *Nat. Struct. Mol. Biol.* 15:675–683.
4. Rothman, J. E. 2014. The principle of membrane fusion in the cell (Nobel lecture). *Angew. Chem. Int. Ed. Engl.* 53:12676–12694.
5. Brunger, A. T. 2005. Structure and function of SNARE and SNARE-interacting proteins. *Q. Rev. Biophys.* 38:1–47.
6. Rizo, J., and C. Rosenmund. 2008. Synaptic vesicle fusion. *Nat. Struct. Mol. Biol.* 15:665–674.
7. Jahn, R., and D. Fasshauer. 2012. Molecular machines governing exocytosis of synaptic vesicles. *Nature.* 490:201–207.
8. Südhof, T. C. 2013. Neurotransmitter release: the last millisecond in the life of a synaptic vesicle. *Neuron.* 80:675–690.
9. Weber, T., B. V. Zemelman, …, J. E. Rothman. 1998. SNAREpins: minimal machinery for membrane fusion. *Cell.* 92:759–772.
10. Schuette, C. G., K. Hatsuzawa, …, R. Jahn. 2004. Determinants of liposome fusion mediated by synaptic SNARE proteins. *Proc. Natl. Acad. Sci. USA.* 101:2858–2863.
11. Zamir, O., and M. P. Charlton. 2006. Cholesterol and synaptic transmitter release at crayfish neuromuscular junctions. *J. Physiol.* 571:83–99.
12. Wasser, C. R., M. Ertunc, …, E. T. Kavalali. 2007. Cholesterol-dependent balance between evoked and spontaneous synaptic vesicle recycling. *J. Physiol.* 579:413–429.
13. Linetti, A., A. Fratangeli, …, P. Rosa. 2010. Cholesterol reduction impairs exocytosis of synaptic vesicles. *J. Cell Sci.* 123:595–605.
14. Churchward, M. A., T. Rogasevskaia, …, J. R. Coorssen. 2005. Cholesterol facilitates the native mechanism of Ca2+-triggered membrane fusion. *J. Cell Sci.* 118:4833–4848.
15. Churchward, M. A., T. Rogasevskaia, …, J. R. Coorssen. 2008. Specific lipids supply critical negative spontaneous curvature—an essential component of native Ca2+-triggered membrane fusion. *Biophys. J.* 94:3976–3986.
16. Churchward, M. A., and J. R. Coorssen. 2009. Cholesterol, regulated exocytosis and the physiological fusion machine. *Biochem. J.* 423:1–14.
17. Chamberlain, L. H., R. D. Burgoyne, and G. W. Gould. 2001. SNARE proteins are highly enriched in lipid rafts in PC12 cells: implications for the spatial control of exocytosis. *Proc. Natl. Acad. Sci. USA.* 98:5619–5624.
18. Lang, T., D. Bruns, …, R. Jahn. 2001. SNAREs are concentrated in cholesterol-dependent clusters that define docking and fusion sites for exocytosis. *EMBO J.* 20:2202–2213.

19. Taverna, E., E. Saba, …, P. Rosa. 2004. Role of lipid microdomains in P/Q-type calcium channel (Cav2.1) clustering and function in presynaptic membranes. *J. Biol. Chem.* 279:5127–5134.

20. Salaün, C., G. W. Gould, and L. H. Chamberlain. 2005. Lipid raft association of SNARE proteins regulates exocytosis in PC12 cells. *J. Biol. Chem.* 280:19449–19453.

21. Salaün, C., G. W. Gould, and L. H. Chamberlain. 2005. The SNARE proteins SNAP-25 and SNAP-23 display different affinities for lipid rafts in PC12 cells. Regulation by distinct cysteine-rich domains. *J. Biol. Chem.* 280:1236–1240.

22. Gil, C., A. Soler-Jover, …, J. Aguilera. 2005. Synaptic proteins and SNARE complexes are localized in lipid rafts from rat brain synaptosomes. *Biochem. Biophys. Res. Commun.* 329:117–124.

23. Lang, T. 2007. SNARE proteins and 'membrane rafts'. *J. Physiol.* 585:693–698.

24. Taverna, E., E. Saba, …, P. Rosa. 2007. Localization of synaptic proteins involved in neurosecretion in different membrane microdomains. *J. Neurochem.* 100:664–677.

25. van den Bogaart, G., T. Lang, and R. Jahn. 2013. Microdomains of SNARE proteins in the plasma membrane. *Curr. Top. Membr.* 72:193–230.

26. Murray, D. H., and L. K. Tamm. 2009. Clustering of syntaxin-1A in model membranes is modulated by phosphatidylinositol 4,5-bisphosphate and cholesterol. *Biochemistry.* 48:4617–4625.

27. Murray, D. H., and L. K. Tamm. 2011. Molecular mechanism of cholesterol- and polyphosphoinositide-mediated syntaxin clustering. *Biochemistry.* 50:9014–9022.

28. Deutsch, J. W., and R. B. Kelly. 1981. Lipids of synaptic vesicles: relevance to the mechanism of membrane fusion. *Biochemistry.* 20:378–385.

29. Thiele, C., M. J. Hannah, …, W. B. Huttner. 2000. Cholesterol binds to synaptophysin and is required for biogenesis of synaptic vesicles. *Nat. Cell Biol.* 2:42–49.

30. Takamori, S., M. Holt, …, R. Jahn. 2006. Molecular anatomy of a trafficking organelle. *Cell.* 127:831–846.

31. Chang, J., S. A. Kim, …, Y. K. Shin. 2009. Fusion step-specific influence of cholesterol on SNARE-mediated membrane fusion. *Biophys. J.* 96:1839–1846.

32. Tong, J., P. P. Borbat, …, Y. K. Shin. 2009. A scissors mechanism for stimulation of SNARE-mediated lipid mixing by cholesterol. *Proc. Natl. Acad. Sci. USA.* 106:5141–5146.

33. Lingwood, D., and K. Simons. 2010. Lipid rafts as a membrane-organizing principle. *Science.* 327:46–50.

34. Simons, K., and M. J. Gerl. 2010. Revitalizing membrane rafts: new tools and insights. *Nat. Rev. Mol. Cell Biol.* 11:688–699.

35. Yeagle, P. L. 1985. Lanosterol and cholesterol have different effects on phospholipid acyl chain ordering. *Biochim. Biophys. Acta.* 815:33–36.

36. Sankaram, M. B., and T. E. Thompson. 1990. Modulation of phospholipid acyl chain order by cholesterol. A solid-state 2H nuclear magnetic resonance study. *Biochemistry.* 29:10676–10684.

37. Recktenwald, D. J., and H. M. McConnell. 1981. Phase equilibria in binary mixtures of phosphatidylcholine and cholesterol. *Biochemistry.* 20:4505–4510.

38. Coorssen, J. R., and R. P. Rand. 1990. Effects of cholesterol on the structural transitions induced by diacylglycerol in phosphatidylcholine and phosphatidylethanolamine bilayer systems. *Biochem. Cell Biol.* 68:65–69.

39. Chen, Z., and R. P. Rand. 1997. The influence of cholesterol on phospholipid membrane curvature and bending elasticity. *Biophys. J.* 73:267–276.

40. Wang, W., L. Yang, and H. W. Huang. 2007. Evidence of cholesterol accumulated in high curvature regions: implication to the curvature elastic energy for lipid mixtures. *Biophys. J.* 92:2819–2830.

41. Bowen, M. E., K. Weninger, …, S. Chu. 2004. Single molecule observation of liposome-bilayer fusion thermally induced by soluble N-ethyl maleimide sensitive-factor attachment protein receptors (SNAREs). *Biophys. J.* 87:3569–3584.

42. Liu, T., W. C. Tucker, …, J. C. Weisshaar. 2005. SNARE-driven, 25-millisecond vesicle fusion in vitro. *Biophys. J.* 89:2458–2472.

43. Yoon, T. Y., B. Okumus, …, T. Ha. 2006. Multiple intermediates in SNARE-induced membrane fusion. *Proc. Natl. Acad. Sci. USA.* 103:19731–19736.

44. Domanska, M. K., V. Kiessling, …, L. K. Tamm. 2009. Single vesicle millisecond fusion kinetics reveals number of SNARE complexes optimal for fast SNARE-mediated membrane fusion. *J. Biol. Chem.* 284:32158–32166.

45. Kiessling, V., B. Liang, and L. K. Tamm. 2015. Reconstituting SNARE-mediated membrane fusion at the single liposome level. *Methods Cell Biol.* 128:339–363.

46. Brunger, A. T., D. J. Cipriano, and J. Diao. 2015. Towards reconstitution of membrane fusion mediated by SNAREs and other synaptic proteins. *Crit. Rev. Biochem. Mol. Biol.* Published online March 19, 2015. http://dx.doi.org/10.3109/10409238.2015.1023252.

47. Domanska, M. K., V. Kiessling, and L. K. Tamm. 2010. Docking and fast fusion of synaptobrevin vesicles depends on the lipid compositions of the vesicle and the acceptor SNARE complex-containing target membrane. *Biophys. J.* 99:2936–2946.

48. Hernandez, J. M., A. J. Kreutzberger, …, R. Jahn. 2014. Variable cooperativity in SNARE-mediated membrane fusion. *Proc. Natl. Acad. Sci. USA.* 111:12037–12042.

49. Fasshauer, D., W. Antonin, …, R. Jahn. 1999. Mixed and non-cognate SNARE complexes. Characterization of assembly and biophysical properties. *J. Biol. Chem.* 274:15440–15446.

50. Fasshauer, D., and M. Margittai. 2004. A transient N-terminal interaction of SNAP-25 and syntaxin nucleates SNARE assembly. *J. Biol. Chem.* 279:7613–7621.

51. Stein, A., A. Radhakrishnan, …, R. Jahn. 2007. Synaptotagmin activates membrane fusion through a Ca2+-dependent trans interaction with phospholipids. *Nat. Struct. Mol. Biol.* 14:904–911.

52. Kiessling, V., S. Ahmed, …, L. K. Tamm. 2013. Rapid fusion of synaptic vesicles with reconstituted target SNARE membranes. *Biophys. J.* 104:1950–1958.

53. Wagner, M. L., and L. K. Tamm. 2001. Reconstituted syntaxin1a/SNAP25 interacts with negatively charged lipids as measured by lateral diffusion in planar supported bilayers. *Biophys. J.* 81:266–275.

54. Wagner, M. L., and L. K. Tamm. 2000. Tethered polymer-supported planar lipid bilayers for reconstitution of integral membrane proteins: silane-polyethyleneglycol-lipid as a cushion and covalent linker. *Biophys. J.* 79:1400–1414.

55. Kalb, E., S. Frey, and L. K. Tamm. 1992. Formation of supported planar bilayers by fusion of vesicles to supported phospholipid monolayers. *Biochim. Biophys. Acta.* 1103:307–316.

56. Hernandez, J. M., A. Stein, …, R. Jahn. 2012. Membrane fusion intermediates via directional and full assembly of the SNARE complex. *Science.* 336:1581–1584.

57. Kiessling, V., J. M. Crane, and L. K. Tamm. 2006. Transbilayer effects of raft-like lipid domains in asymmetric planar bilayers measured by single molecule tracking. *Biophys. J.* 91:3313–3326.

58. Bartlett, G. R. 1959. Phosphorus assay in column chromatography. *J. Biol. Chem.* 234:466–468.

59. Pokorny, A., T. H. Birkbeck, and P. F. Almeida. 2002. Mechanism and kinetics of delta-lysin interaction with phospholipid vesicles. *Biochemistry.* 41:11044–11056.

60. Kiessling, V., M. K. Domanska, and L. K. Tamm. 2010. Single SNARE-mediated vesicle fusion observed in vitro by polarized TIRFM. *Biophys. J.* 99:4047–4055.

61. Wang, T., E. A. Smith, …, J. C. Weisshaar. 2009. Lipid mixing and content release in single-vesicle, SNARE-driven fusion assay with 1-5 ms resolution. *Biophys. J.* 96:4122–4131.

62. Rawle, R. J., B. van Lengerich, …, S. G. Boxer. 2011. Vesicle fusion observed by content transfer across a tethered lipid bilayer. *Biophys J.* 101:L37–L39.

63. van Lengerich, B., R. J. Rawle, P. M. Bendix, and S. G. Boxer. 2013. Individual vesicle fusion events mediated by lipid-anchored DNA. *Biophys J.* 105:409–419.

64. Bradford, A., J. Atkinson, …, R. P. Rand. 2003. The effect of vitamin E on the structure of membrane lipid assemblies. *J. Lipid Res.* 44:1940–1945.

65. Mitter, D., C. Reisinger, …, G. Ahnert-Hilger. 2003. The synaptophysin/synaptobrevin interaction critically depends on the cholesterol content. *J. Neurochem.* 84:35–42.

66. Huttner, W. B., and A. Schmidt. 2000. Lipids, lipid modification and lipid-protein interaction in membrane budding and fission—insights from the roles of endophilin A1 and synaptophysin in synaptic vesicle endocytosis. *Curr. Opin. Neurobiol.* 10:543–551.

67. Wan, C., V. Kiessling, …, L. K. Tamm. 2011. Partitioning of synaptotagmin I C2 domains between liquid-ordered and liquid-disordered inner leaflet lipid phases. *Biochemistry.* 50:2478–2485.

68. Lv, J. H., L. He, and S. F. Sui. 2008. Lipid rafts association of synaptotagmin I on synaptic vesicles. *Biochemistry (Mosc.).* 73:283–288.

69. Kato, N., M. Nakanishi, and N. Hirashima. 2003. Cholesterol depletion inhibits store-operated calcium currents and exocytotic membrane fusion in RBL-2H3 cells. *Biochemistry.* 42:11808–11814.

70. Liang, B., D. Dawidowski, …, D. S. Cafiso. 2014. The SNARE motif of synaptobrevin exhibits an aqueous-interfacial partitioning that is modulated by membrane curvature. *Biochemistry.* 53:1485–1494.

71. Liang, B., V. Kiessling, and L. K. Tamm. 2013. Prefusion structure of syntaxin-1A suggests pathway for folding into neuronal trans-SNARE complex fusion intermediate. *Proc. Natl. Acad. Sci. USA.* 110:19384–19389.

72. Yang, L., and H. W. Huang. 2002. Observation of a membrane fusion intermediate structure. *Science.* 297:1877–1879.

73. Aeffner, S., T. Reusch, …, T. Salditt. 2012. Energetics of stalk intermediates in membrane fusion are controlled by lipid composition. *Proc. Natl. Acad. Sci. USA.* 109:E1609–E1618.

74. Chernomordik, L. V., and M. M. Kozlov. 2005. Membrane hemifusion: crossing a chasm in two leaps. *Cell.* 123:375–382.

75. Otterstrom, J., and A. M. van Oijen. 2013. Visualization of membrane fusion, one particle at a time. *Biochemistry.* 52:1654–1668.

76. Kyoung, M., A. Srivastava, …, A. T. Brunger. 2011. In vitro system capable of differentiating fast Ca2+-triggered content mixing from lipid exchange for mechanistic studies of neurotransmitter release. *Proc. Natl. Acad. Sci. USA.* 108:E304–E313.